ACS OMEGA

Open Access

http://pubs.acs.org/journal/acsodf

Article

Solid-State Synthesis of Niobium Carbide Electrocatalyst in the Presence of Vanadium as Suppressor of Energy Input and Greenhouse Gas Emission

Kenji Saito,* Takahiro Jinushi, and Itsuki Soga

Cite This: *ACS Omega* 2024, 9, 7069−7074

Read Online

ACCESS | Metrics & More | Article Recommendations | Supporting Information

ABSTRACT: Solid-state reaction (SSR) is a widely adopted method for functional inorganic material syntheses. Unlike intricate systems emerging from chemically unstable precursor usage, the SSR can proceed from stable precursor couples using simple apparatuses. However, this reaction is associated with high temperatures that overcome solid-state diffusion. Moreover, solid-state syntheses of technologically crucial carbides lead to greenhouse gas emissions. Therefore, exploring an extrinsic component to suppress these challenges is vital to confronting global energy and environmental issues. This study reports that the presence of an ordinary element, vanadium (V), changes the routes of the SSR of niobium carbide (NbC), producing NbC efficiently and cleanly. 1000 °C is far below the temperature required to obtain NbC from a precursor couple of Nb_2O_5 and C, i.e., approximately 1500 °C is required. However, a carbon substitute, vanadium carbide, completely consumed Nb_2O_5 before reaching 1000 °C and consummated NbC crystallization for 10 h. Furthermore, NbC crystallites were observed using X-ray diffraction from 770 °C, and their formation was primarily accompanied by $VNbO_4$, rather than being routed through NbO_2 produced for the Nb_2O_5−C combination. The obtained NbC contained V as a dopant in the 15−50% range (NbC:V), and the relative abundance was correlated with the preparation temperature. Mass analyses revealed that the formation of NbC/V is barely associated with greenhouse gas emissions because of the sizable thermodynamic driving force for primarily forming vanadium oxide byproducts. Device performance using NbC/V was also assessed for a standard electrochemical hydrogen evolution reaction.

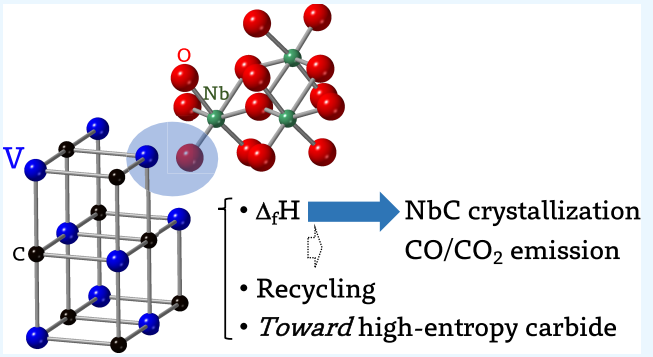

INTRODUCTION

Solid-state reaction (SSR) is a widely adopted approach for inorganic functional material syntheses. SSR can proceed from chemically stable precursor couples in simple apparatuses,[1] and hence holding down initial investments to execute experiments and the related electric power consumption. However, the reaction requires high temperatures to overcome energy barriers for solid-state diffusion.[2,3] Conversely, the solid-state metathesis (SSM) reaction occurs with lower energy barriers.[4−6] The driving force of SSM originates from the enormous formation energies of byproducts, such as alkali and alkaline-earth halides. The typical precursors, metal chlorides, frequently show vapor-pressures at low temperatures,[7] leading to a phase change and facilitating a self-propagation reaction.[5] Moreover, the metal chloride precursors are often highly oxidative, hence, imposing the construction of intricate experimental systems. Todd and Neilson reported that the precursor of SSM, alkali species, modifies reaction pathways, enabling low temperature syntheses of yttrium manganese oxides.[8] Herein, the modification of reaction routes with extrinsic components may occur in halide-free SSR systems.

SSR and SSM have been frequently used for the syntheses of refractory and superhard materials, including pnictides, chalcogenides, silicides, borides, and carbides.[9] Carbides in which carbon atoms are dissolved in interstitial sites of early transition metals show properties suitable for industrial utilization in terms of hardness, melting point, conductivity, and chemical stability.[10,11] Niobium carbide (NbC) stands out owing to its capabilities as an electrocatalyst for fuels—a cathode of electrochemical water splitting[12−19] and the latent ability to reduce CO_2.[20] SSR of NbC has been performed using Nb_2O_5 and carbon sources, such as C.[10,11] The reaction necessitates high temperatures and results in greenhouse gas emissions. To overcome these challenges, the extrinsic component that is incorporated in SSR must prefer oxygen

Received: November 13, 2023
Revised: January 16, 2024
Accepted: January 22, 2024
Published: January 31, 2024

atoms rather than carbon atoms. In addition, the resulting oxide byproduct must show sufficient formation enthalpy to facilitate SSR, and it must be easier to separate from the product.

Vanadium (V) is the recognized important material in strategic industries,[21] and its utilization as a precursor has been primarily investigated in engineering steels (an alloying element in steels).[22−26] V forms highly stable oxides rather than carbon oxides [standard enthalpy of formation, $\Delta_f H°$/kJ mol^{-1}: CO (−110.5), CO_2 (−393.5), V_2O_3 (−1219), V_2O_5 (−1550)].[27] Furthermore, the V oxides can dissolve in various solutions and are easily recyclable. Therefore, V is a candidate as an extrinsic component for the improved SSR synthesis of NbC.

This study describes the utilization of V as a significant component to stably carry carbon atoms and produce a significant amount of reaction heat when it reconstructs the chemical bonds with the oxygen atoms contained in Nb_2O_5. The vanadium carbide (VC) precursor, a rare carbides preparable with CO_2 as a feed,[28] does not undergo a topotactic process with Nb_2O_5 but instead alters chemical reaction routes in Nb_2O_5−C. The mechanistic aspects and the obtained NbC performance are investigated.

RESULTS AND DISCUSSION

The X-ray diffraction (XRD) profiles shown in Figure 1 compare the products obtained from the SSR (at 1000 °C for 10 h) of Nb_2O_5 with typical C or VC. The former only produced reduced niobium oxides, such as NbO_2 and $Nb_{12}O_{29}$, even if molar ratios of C to Nb_2O_5 increased. The reported synthesis temperature of the couple reaches as high as 1500 °C.[11] Conversely, using VC instead of C resulted in the formation of NbC with $VNbO_4$ and V_2O_3. The $VNbO_4$ formation is correlated with kinetic factors, i.e., for 10 h heating, the XRD peak intensities decrease with increasing temperature or molar ratios [VC]/[Nb_2O_5], indicating that $VNbO_4$ is a reaction intermediate (Figure S1). Figures 2 and S2 show, using separate diffraction lines, a qualitative temporal transition of each chemical species involved in the reaction, in which each reaction, except for 10 h, is terminated by quenching in air. The expense of VC is accompanied by the formation of NbC and V_2O_3, indicating that they are correlative. On the other hand, for $VNbO_4$, the peak heights once increase (Figure 2a), but the integrated intensities (Figure 2b) monotonically decrease. This suggests an improvement in crystallinity after exposure to heat for a longer time. Furthermore, note that no signal of Nb_2O_5 was observed even for 0.01 h; it is completely consumed on heating—less than 2 h—to produce NbC and/or $VNbO_4$.

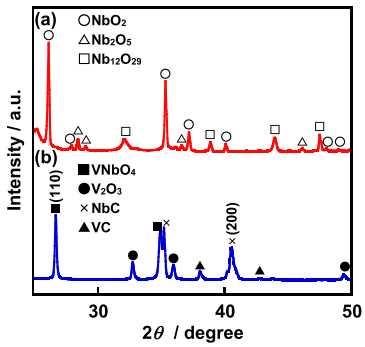

Figure 1. XRD patterns of products obtained from (a) Nb_2O_5−C and (b) Nb_2O_5−VC at 1000 °C for 10 h. Each symbol indicates NbO_2 (PDF 82-1141), Nb_2O_5 (PDF 27-1003), $Nb_{12}O_{29}$ (PDF 75-2949), NbC (PDF 74-1222), VC (PDF 74-1220), $VNbO_4$ (PDF 74-6531), and V_2O_3 (PDF 71-0344). Molar ratios are as follows: [C]/[Nb_2O_5] = 7; [VC]/[Nb_2O_5] = 2.

The products other than NbC after 10 h of heating are V_2O_3 and VC, and stirring in nitric acid easily removes them. The HNO_3-treated product shows only reflections of NbC (Figure S3). However, each peak is broadened and shifted toward higher Bragg angles, compared with those of the other byproducts and PDF 74-1222 of NbC. To investigate the former, crystallite size D[29] and lattice distortion ε, computed using the Williamson−Hall method,[30] are compared with those of phase-pure NbC prepared by heating C and Nb_2O_5 at 1450 °C (hereinafter, only the carbon source used is described before parentheses of values for simplification). The obtained ε % [C (0.072), VC (0.56)] and D/Å [C (533.5), VC (286)] suggest that crystallite size, rather than lattice distortion, is the primary cause of broadening. Meanwhile, according to Bragg's law[31] the shift of the observed XRD peak toward a higher angle is a Nb-to-V atomic displacement in NbC [ionic radius for six coordination/Å, V^{4+} (0.58), Nb^{4+} (0.68)]. Elemental analysis using energy-dispersive X-ray spectroscopy equipped with scanning electron microscopy (SEM−EDS) reveals, in NbC prepared from VC, the presence of V, representing 15% of Nb. The refined lattice parameters and cell volumes, using the Rietveld method, are as follows: a/Å [C (4.45193(9)), VC (4.44280(11))] and V/Å^3 [C (88.236(3)), VC (87.694(4))]. The decreased lattice constant, by replacing C with VC, is consistent with the positive XRD peak shift, and the result is also supported by density functional theory (DFT) calculations. That is, the structure optimization of $Nb_{0.85}V_{0.15}C$ (15% of Nb sites are substituted with V) shows results similar to those of the Rietveld analyses (Table S1). Therefore, V was found to substitute Nb in NbC during SSR. In the Raman spectrum of less than 1100 cm^{-1} (Figure S4a), the obtained V substitute, NbC/V, exhibits three NbC phonon spectra, including its acoustic and optical parts.[32] Among them, a peak at 980 cm^{-1} shows a pronounced negative shift compared with that of pure NbC, implying changes in Nb−C bonds by the V substitution. Meanwhile, no signal was detected in a wavenumber range of 1200−1700 cm^{-1} (Figure S4b), which corresponds to the region of G and D bands found in carbon deposits, such as graphites, and has been a subject of research on prepared NbC.[16,17,33] Figure 3 and Table 1 describe a relationship between the temperature added to Nb_2O_5−VC and the relative abundance of NbC to internal standard Si (NIST 640d), determined using XRD peak ratios, or physical properties of NbC. In contrast to others, 1200 °C heating results in peak splitting, which is fitted to two components of NbC (Figure S5). In the single-component heating regions being studied, the occupancy of V, obtained from Rietveld analyses, correlates with that of EDS (Figure S6) and thus applies to those of 1200 °C. As a simplified tendency, we observe that temperature rise increases vanadium concentrations of NbC/V to a maximum of 47.9(52)%, and the progress of the substitution decreases the lattice constants a and D and conversely increases ε, indicating that V hinders the crystal growth of NbC by increased distortion in its crystallites. It possibly underestimates the formation temperature of NbC; its crystallites may be formed from 700 °C identical to that of $VNbO_4$ (Figure S5).

https://doi.org/10.1021/acsomega.3c09045
ACS Omega 2024, 9, 7069−7074

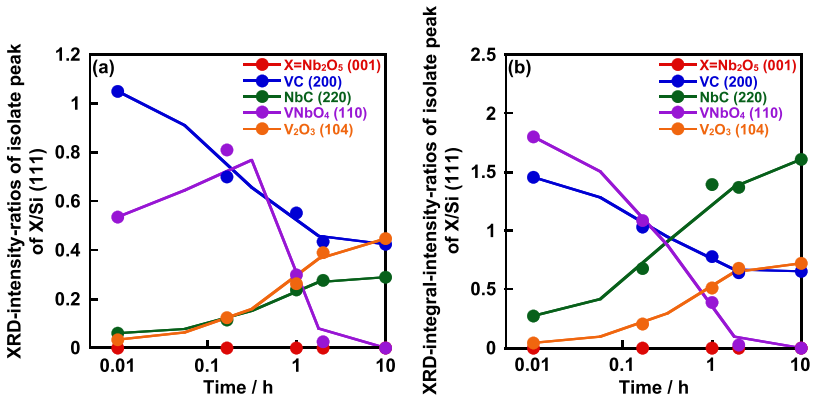

Figure 2. Plots of reaction time vs. (a) XRD intensity ratios of isolate peak of material to (111) of Si and (b) modification of (a) by replacing the intensity ratio with integral intensity ratio. The three-digit number in the bracket indicates Miller indices of isolate peaks of each material.

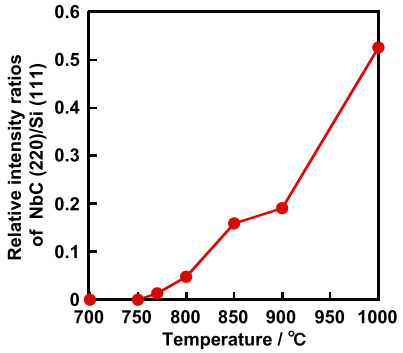

Figure 3. Onset temperature of formation of NbC crystallites, using relative intensity ratios of (220) NbC to (111) Si.

The reaction intermediate of Nb_2O_5 with C has been reported to be NbO_2;[10] however, although the SSR of Nb_2O_5−VC is performed in a short time or at low temperatures (Figure 2), the species is not observed, suggesting a different reaction mechanism. When NbO_2 was reacted with VC at 1000 °C for 10 h, which is a sufficient time to completely consume $VNbO_4$, NbO_2 remained (Figure S7), indicating that NbO_2 is not a necessary intermediate to yield NbC. Although NbO_2 is formed by the reduction of Nb_2O_5, $VNbO_4$ has V^{III} and Nb^{V},[34] whose valence states are included in VC[35,36] and identical to Nb_2O_5. The closer relationship between constituent ions prioritizes the formation of $VNbO_4$ over NbO_2. As shown in Figure 2, $VNbO_4$ and V_2O_3 are byproducts observable using XRD; however, the formation of V_2O_5 is visually detected as well, i.e., a reaction tube was colored pale orange[37] by sublimation.

Thus, the following primary chemical reactions are expected in the presence of VC.

$$Nb_2O_5 + 2VC \rightarrow 2NbC + V_2O_3 + O_2 \quad (1)$$

$$Nb_2O_5 + VC \rightarrow NbC + VNbO_4 + \frac{1}{2}O_2 \quad (1\text{-}1)$$

$$VNbO_4 + VC \rightarrow NbC + V_2O_3 + \frac{1}{2}O_2 \quad (1\text{-}2)$$

where the overall reaction eq 1 is the sum of the half-reactions 1-1 and 1-2.

$$Nb_2O_5 + 2VC \rightarrow 2NbC + V_2O_5 \quad (2)$$

Gas emission was evaluated using the weight loss of a pellet associated with SSR, rather than using a gas chromatograph. This is because in a constantly flowing inert gas accurately quantifying any component with low partial pressure is difficult. As a result, the reference system, Nb_2O_5−C, lost 41.2% of its weight after SSR, which is close to the CO percent by mass (40.0%) for the following reaction: $Nb_2O_5 + 7C \rightarrow 2NbC + 5CO$.[11] Conversely, the Nb_2O_5−VC system, computed after 1000 °C heating for 10 h, decreased by only 5.13%. Equation 1 will lose its weight with O_2 emission by 5.51%, which is larger than the result of our experiments. The probable reasons for this are the contribution of eq 2 and the adsorption of O_2 into carbides. Although the emission of CO/CO_2 for Nb_2O_5−VC is not zero, i.e., discharged fluids slightly make a $Ca(OH)_2$ aqueous solution cloudy,[38] using VC as a substitute for C was found to drastically reduce CO/CO_2 emissions during the NbC synthesis. Meanwhile, both NbC and VC have a NaCl-type structure,[11] and the small lattice mismatch, i.e., the lattice constant a/Å = 4.4686 (NbC) and 4.1629 (VC), and the presence of congeneric cations suggest the possibility of a topotactic reaction, where a structure motif is kinetically inserted or deserted while preserving the intrinsic structures of parent materials.[39] Figure S8 compares field

Table 1. Summary of Physical Properties of Obtained NbC—Lattice Constant a, Crystallite Size D, Lattice Distortion ε, and Values of V of Site Occupancy and Atom % Obtained Using EDS

combination	temperature/°C	a/Å	D/Å	ε	occupancy	atom %
Nb_2O_5−VC	1000	4.44280(11)	286(2)	0.56(2)	0.215(15)	16.6(13)
	1100	4.42970(8)	188.8(13)	0.49(5)	0.320(13)	20.8(22)
	1200(L)	4.37479(11)	417(2)	0.979(5)	0.39(5)	29.9(34)
	1200(H)	4.2145(5)	101.1(4)	0.41(14)	0.3(6)	29.9(34)
	1300	4.3412(4)	125.3(3)	0.73(3)	0.39(2)	47.9(52)
Nb_2O_5−C	1450	4.45193(9)	533.5(9)	0.072(12)		

https://doi.org/10.1021/acsomega.3c09045
ACS Omega 2024, 9, 7069−7074

emission SEM (FE-SEM) images of Nb_2O_5, VC, and the product NbC/V. There is no correlation between particle sizes and shapes. Therefore, a contribution is not likely. Meanwhile, as VB TMCs (VC, NbC, and TaC) have similar bonding enthalpies,[40−42] the primary thermodynamic driving force for Nb_2O_5−VC[5,6] stems from a difference in the formation heat between Nb_2O_5 and the resulting vanadium oxides [standard enthalpy of formation [$\Delta_f H°$/kJ mol^{-1}: Nb_2O_5 (−1900), V_2O_3 (−1219), V_2O_5 (−1550)].[27] The endothermic energies are less than those for Nb_2O_5−C (Nb_2O_5 + 7C → 2NbC + 5CO). Finally, standard electrochemical hydrogen evolution reactions (HER) were performed to investigate the effects of V introduced into the NbC lattices. Table S2 summarizes the recent HER performance of NbC and its related systems. The overpotentials, Tafel slopes, double layer capacitance C_{dl}, and lowest charge transfer resistance R_{CT} are given in Table S2 were obtained from Figure 4. The overpotential of pure NbC

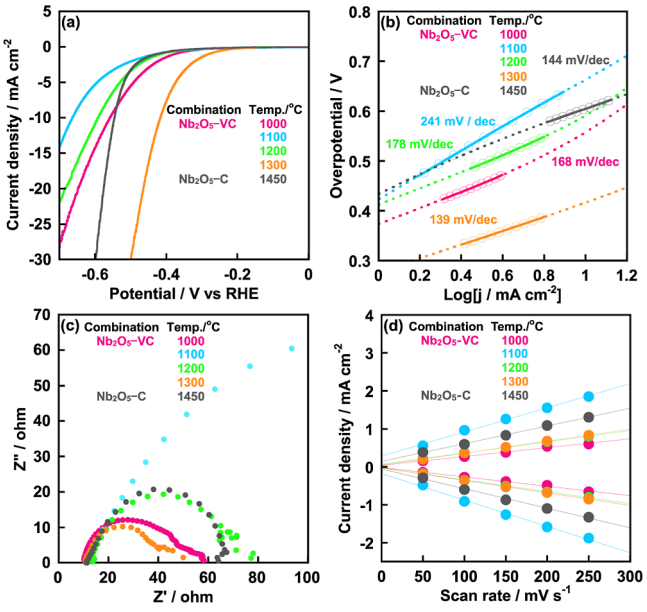

Figure 4. (a) Linear sweep voltammograms, (b) Tafel plots, (c) Nyquist plots, and (d) cathodic and anodic non-Faradaic capacitive currents at 0 V (vs SCE) against scan rates of the obtained NbC/V electrodes and reference (NbC). Precursor combination and the preparation temperatures are described in each figure using different colors, and the color coding of each sample is standardized between figures. Characters with units (mV/dec) near straight lines indicate Tafel slopes.

(entry 5) belongs to those of entries 6 and 10; therefore, this compound can be regarded as a reference. V under 30% (entries 1 and 3, Table 1) has almost no impact on the overpotential of entry 5. However, the heaviest V (entry 4) considerably enhances the performance. The correlation of only R_{CT} demonstrates that the enhanced HER performance is due to charge transfer rather than the active surface area (C_{dl}). The recent reports are also suggestive that a combination with rGO or the relevant conductive materials further improves the HER performance of NbC/V.

CONCLUSIONS

Two SSR systems for the synthesis of the NbC electrocatalysts, Nb_2O_5−C and Nb_2O_5−VC, were compared to investigate the effects of vanadium(V). Each stable precursor couple is seemingly similar, but the chemical reactions vary significantly. Under heating, V promptly reconstructed chemical bonds with oxygens in Nb_2O_5, suppressing greenhouse gas emissions and releasing enormous reaction enthalpies, which contributed to reducing the temperature of reaction completion from 1450 to 1000 °C, as well as facilitating NbC crystallization (770 °C). The primary reaction intermediate is altered from NbO_2 (for Nb_2O_5−C) to $VNbO_4$, which is also regarded as a cause of temperature depression. NbC contains V in the crystal lattice; however, its presence is controllable by temperature and in a highly doped region, which is favorable to HER performance. Furthermore, the atomic mixing to near-equimolar ratios is thought to be applicable to the fields of high-entropy carbides studied at high temperatures.[43,44] Although precursor utilization of V has thus far been primarily investigated in engineering steels (an alloying element in steels), this study may broaden the application areas.

EXPERIMENTAL SECTION

Characterizations were performed by using the following facilities: XRD using Cu Kα as an X-ray source (Rigaku MiniFlex600); FE-SEM (JEOL JSM-6500F); SEM−EDS (JEOL JSM-6510LV); Raman spectroscopy using a 532 nm laser (Horiba LabRAM HR-800); Potentiostat (BAS ALS-644D), and gas chromatography (Shimadzu GC-8A).

Protocols for SSR. In an agate mortar, Nb_2O_5 (0.953 mmol) and several times the molar quantity of VC are mixed in air and pressed with a pump pressure of 60 MPa into a 13 mm-diameter pellet. The pellet was placed on a Pt foil or a C sheet and put in an alumina Tamman tube before being positioned at the center of a cylindrical alumina tube (24 mm diameter and 600 mm long) of a furnace. Twenty-five mL min^{-1} Ar was introduced from an open-ended side of the Tamman tube 20 min before the furnace launched a heating program with a ramp rate of 7 °C min^{-1}. Nb_2O_5 and C were reacted using the same protocol of Nb_2O_5−VC, as the reference. For investigations of chemical species at fixed intervals (Figure 2), quenching was performed by immediately transferring the interior Tamman tube to an ambient temperature region from the heating furnace.

Performance Assessment by HER. A three-electrode system consisting of a working electrode, a counter electrode (3 mmϕ carbon-rod), and a saturated calomel electrode as a reference, was employed to assess the HER of the obtained NbC/V. The working electrode was prepared according to previous reports.[45] A mixture of NbC/V or pure NbC (5 mg), carbon black (5 mg), 2-propanol (400 μL), 5 wt % Nafion solution (30 μL), and ultrapure water (600 μL) was placed in an ultrasonic bath for 30 min to obtain an NbC ink. The ink was drop-cast on a 3 mmϕ glassy carbon electrode and dried in air. The HER was performed in a 0.5 mol L^{-1} H_2SO_4 electrolyte.

Theoretical Method. Quantum Espresso, a DFT software package, was used to optimize the geometries of $Nb_{0.85}V_{0.15}C$ and NbC. The kinetic energy cutoff (E_{cut} = 60 Ry) and k-point mesh (a 4 × 4 × 4 grid) were used.

ASSOCIATED CONTENT

Supporting Information

The Supporting Information is available free of charge at https://pubs.acs.org/doi/10.1021/acsomega.3c09045.

https://doi.org/10.1021/acsomega.3c09045
ACS Omega 2024, 9, 7069−7074

Time and temperature evolutions of Nb_2O_5−VC and the reference reactions (Figures S1−S3, S5−S7), Raman spectroscopy (S4), V analyses (S6), and FE-SEM observation (S8) for characterizations of reaction products, DFT calculations for structure optimization (Table S1), and HER performance comparison (Table S2) (PDF)

AUTHOR INFORMATION

Corresponding Author

Kenji Saito − *Department of Materials Science and Technology, Faculty of Engineering, Niigata University, Niigata 950-2181, Japan;* orcid.org/0009-0001-9921-0109; Email: ksaito@eng.niigata-u.ac.jp

Authors

Takahiro Jinushi − *Department of Materials Science and Technology, Faculty of Engineering, Niigata University, Niigata 950-2181, Japan*

Itsuki Soga − *Department of Materials Science and Technology, Faculty of Engineering, Niigata University, Niigata 950-2181, Japan*

Complete contact information is available at: https://pubs.acs.org/10.1021/acsomega.3c09045

Notes

The authors declare no competing financial interest.

ACKNOWLEDGMENTS

K.S. acknowledges financial support from the Sasaki Environment Technology Foundation, Iwatani Naoji Foundation, Takahashi Industrial and Economic Research Foundation, Tanikawa Fund Promotion of Thermal Technology, and Amano Institute of Technology.

REFERENCES

(1) Buekenhoudt, A.; Kovalevsky, A.; Luyten, J.; Snijkers, F. Basic Aspects in Inorganic Membrane Preparation. In *Comprehensive Membrane Science and Engineering*, 1st ed.; Drioli, E., Giorno, L., Eds.; Elsevier, 2010; pp 217−252.

(2) Disalvo, F. J. Solid-State Chemistry: A Rediscovered Chemical Frontier. *Science* **1990**, *247*, 649−655.

(3) Kumar, A.; Dutta, S.; Kim, S.; Kwon, T.; Patil, S. S.; Kumari, N.; Jeevanandham, S.; Lee, I. S. Solid-State Reaction Synthesis of Nanoscale Materials: Strategies and Applications. *Chem. Rev.* **2022**, *122*, 12748−12863.

(4) Parkin, I. P.; Kafizas, A. Exothermic Metathesis Reactions. In *Comprehensive Inorganic Chemistry II*; Reedijk, J., Poeppelmeier, K., Eds.; Elsevier, 2013; pp 471−490.

(5) Gillan, E. G.; Kaner, R. B. Synthesis of Refractory Ceramics via Rapid Metathesis Reactions between Solid-State Precursors. *Chem. Mater.* **1996**, *8*, 333−343.

(6) Wiley, J. B.; Kaner, R. B. Rapid Solid-State Precursor Synthesis of Materials. *Science* **1992**, *255*, 1093−1097.

(7) Sadoway, D. R.; Flengas, S. N. Vapour Pressures of Solid and Liquid $NbCl_5$ and $TaCl_5$. *Can. J. Chem.* **1976**, *54*, 1692−1699.

(8) Todd, P. K.; Neilson, J. R. Selective Formation of Yttrium Manganese Oxides through Kinetically Competent Assisted Metathesis Reactions. *J. Am. Chem. Soc.* **2019**, *141*, 1191−1195.

(9) Patil, K. C.; Aruna, S. T.; Ekambaram, S. Combustion Synthesis. *Curr. Opin. Solid State Mater. Sci.* **1997**, *2*, 158−165.

(10) Teixeira da Silva, V.; Schmal, M.; Oyama, S. T. Niobium Carbide Synthesis from Niobium Oxide: Study of the Synthesis Conditions, Kinetics, and Solid-State Transformation Mechanism. *J. Solid State Chem.* **1996**, *123*, 168−182.

(11) Oyama, S. T. Introduction to the Chemistry of Transition Metal Carbides and Nitrides. In *The Chemistry of Transition Metal Carbides and Nitrides*; Oyama, S. T., Ed.; Springer Nature, 1996; pp 1−27.

(12) Liu, Y.; Kelly, T. G.; Chen, J. G.; Mustain, W. E. Metal Carbides as Alternative Electrocatalyst Supports. *ACS Catal.* **2013**, *3*, 1184−1194.

(13) Kimmel, Y. C.; Xu, X.; Yu, W.; Yang, X.; Chen, J. G. Trends in Electrochemical Stability of Transition Metal Carbides and Their Potential Use as Supports for Low-Cost Electrocatalysts. *ACS Catal.* **2014**, *4*, 1558−1562.

(14) Yate, L.; Emerson Coy, L.; Wang, G.; Beltrán, M.; Díaz-Barriga, E.; Saucedo, E. M.; Ceniceros, M. A.; Załęski, K.; Llarena, I.; Möller, M.; Ziolo, R. F. Tailoring Mechanical Properties and Electrical Conductivity of Flexible Niobium Carbide Nanocomposite Thin Films. *RSC Adv.* **2014**, *4*, 61355−61362.

(15) Meyer, S.; Nikiforov, A. V.; Petrushina, I. M.; Köhler, K.; Christensen, E.; Jensen, J. O.; Bjerrum, N. J. Transition Metal Carbides (WC, Mo_2C, TaC, NbC) as Potential Electrocatalysts for the Hydrogen Evolution Reaction (HER) at Medium Temperatures. *Int. J. Hydrogen Energy* **2015**, *40*, 2905−2911.

(16) Coy, E.; Yate, L.; Valencia, D. P.; Aperador, W.; Siuzdak, K.; Torruella, P.; Azanza, E.; Estrade, S.; Iatsunskyi, I.; Peiro, F.; et al. High Electrocatalytic Response of a Mechanically Enhanced NbC Nanocomposite Electrode toward Hydrogen Evolution Reaction. *ACS Appl. Mater. Interfaces* **2017**, *9*, 30872−30879.

(17) Gupta, A.; Mittal, M.; Singh, M. K.; Suib, S. L.; Pandey, O. P. Low Temperature Synthesis of NbC/C Nano-Composites as Visible Light Photoactive Catalyst. *Sci. Rep.* **2018**, *8*, 13597.

(18) Gao, Q.; Zhang, W.; Shi, Z.; Yang, L.; Tang, Y. Structural Design and Electronic Modulation of Transition-Metal-Carbide Electrocatalysts toward Efficient Hydrogen Evolution. *Adv. Mater.* **2019**, *31*, No. e1802880.

(19) Chebanenko, M. I.; Danilovich, D. P.; Lobinsky, A. A.; Popkov, V. I.; Rempel, A. A.; Valeeva, A. A. Novel High Stable Electrocatalyst based on Non-Stoichiometric Nanocrystalline Niobium Carbide toward Effective Hydrogen Evolution. *Int. J. Hydrogen Energy* **2021**, *46*, 16907−16916.

(20) Sarabadani Tafreshi, S.; Ranjbar, M.; Taghizade, N.; Panahi, S.; Jamaati, M.; de Leeuw, N. H. A First-Principles Study of CO_2 Hydrogenation on a Niobium-Terminated NbC (111) Surface. *ChemPhysChem* **2022**, *23*, No. e202100781.

(21) Petranikova, M.; Tkaczyk, A. H.; Bartl, A.; Amato, A.; Lapkovskis, V.; Tunsu, C. Vanadium Sustainability in the Context of Innovative Recycling and Sourcing Development. *Waste Manage.* **2020**, *113*, 521−544.

(22) Lagneborg, R.; Siwecki, T.; Zajac, S. Role of Vanadium in Microalloyed Steels. *Scand. J. Metall.* **1999**, *28*, 186−241.

(23) Feng, P.; He, Y.; Xiao, Y.; Xiong, W. Effect of VC Addition on Sinterability and Microstructure of Ultrafine Ti(C, N)-Based Cermets in Spark Plasma Sintering. *J. Alloys Compd.* **2008**, *460*, 453−459.

(24) Qi, X.; Jia, Z.; Yang, Q.; Yang, Y. Effects of Vanadium Additive on Structure Property and Tribological Performance of High Chromium Cast Iron Hardfacing Metal. *Surf. Coat. Technol.* **2011**, *205*, 5510−5514.

(25) Yang, G.; Sun, X.; Li, Z.; Li, X.; Yong, Q. Effects of Vanadium on the Microstructure and Mechanical Properties of a High Strength Low Alloy Martensite Steel. *Mater. Des.* **2013**, *50*, 102−107.

(26) Ren, J.-k.; Chen, Q.-y.; Chen, J.; Liu, Z.-y. Role of Vanadium Additions on Tensile and Cryogenic-Temperature Charpy Impact Properties in Hot-Rolled High-Mn Austenitic Steels. *Mater. Sci. Eng., A* **2021**, *811*, 141063.

(27) Standard Thermodynamic Properties of Chemical Substances. In *CRC Handbook of Chemistry and Physics*, 92nd ed.; Haynes, W. M., Ed.; CRC Press, 2011; pp 5-4−5-42.

(28) Chen, Y.; Wang, M.; Lv, A.; Zhao, Z.; An, J.; Zhang, J.; Tu, J.; Jiao, S. Green Preparation of Vanadium Carbide through One-Step Molten Salt Electrolysis. *Ceram. Int.* **2021**, *47*, 28203−28209.

(29) Holder, C. F.; Schaak, R. E. Tutorial on Powder X-ray Diffraction for Characterizing Nanoscale Materials. *ACS Nano* **2019**, *13*, 7359−7365.
(30) Nath, D.; Singh, F.; Das, R. X-Ray Diffraction Analysis by Williamson-Hall, Halder-Wagner and Size-Strain Plot Methods of CdSe Nanoparticles- A Comparative Study. *Mater. Chem. Phys.* **2020**, *239*, 122021.
(31) Waseda, Y.; Matsubara, E.; Shinoda, K. Scattering and Diffraction. In *X-ray Diffraction Crystallography*; Springer, 2011; pp 67−80.
(32) Spengler, W.; Kaiser, R. First and Second Order Raman Scattering in Transition Metal Compounds. *Solid State Commun.* **1976**, *18*, 881−884.
(33) Mahle, R.; Mahapatra, P. L.; Singh, A. K.; Kumbhakar, P.; Paliwal, M.; Tiwary, C. S.; Banerjee, R. Anaerobe Syntrophic Co-Culture-Mediated Green Synthesis of Ultrathin Niobium Carbide (NbC) Sheets for Flexoelectricity Generation. *ACS Sustain. Chem. Eng.* **2022**, *10*, 13650−13660.
(34) Oppermann, H.; von Woedtke, F.; Reich, T.; Denecke, M. A.; Nitsche, H.; Doerr, M. Phase Relations in the System V/Nb/O. V. Investigation of Mixed Crystals $V_{1-x}Nb_xO_2$. *Fresenius. J. Anal. Chem.* **1999**, *363*, 202−205.
(35) Ramqvist, L.; Hamrin, K.; Johansson, G.; Fahlman, A.; Nordling, C. Charge Transfer in Transition Metal Carbides and Related Compounds Studied by ESCA. *J. Phys. Chem. Solids* **1969**, *30*, 1835−1847.
(36) Ramqvist, L.; Hamrin, K.; Johansson, G.; Gelius, U.; Nordling, C. VC, NbC and TaC with Varying Carbon Content Studied by ESCA. *J. Phys. Chem. Solids* **1970**, *31*, 2669−2672.
(37) Shyrokykh, T.; Wei, X.; Seetharaman, S.; Volkova, O. Vaporization of Vanadium Pentoxide from $CaO-SiO_2-VO_x$ Slags during Alumina Dissolution. *Metall. Mater. Trans. B* **2021**, *52*, 1472−1483.
(38) Atkins, P.; Overton, T.; Rourke, J.; Weller, M.; Armstrong, F. The Group 2 Elements. In *Shriver and Atkins Inorganic Chemistry*, 5th ed.; Oxford University Press, 2006; pp 309−324.
(39) Gabilondo, E.; O'Donnell, S.; Newell, R.; Broughton, R.; Mateus, M.; Jones, J. L.; Maggard, P. A. Renaissance of Topotactic Ion-Exchange for Functional Solids with Close Packed Structures. *Chem. Eur. J.* **2022**, *28*, No. e202200479.
(40) Kurlov, A. S.; Gusev, A. I. High-Energy Milling of Non-stoichiometric Carbides: Effect of Nonstoichiometry on Particle Size of Nanopowders. *J. Alloys Compd.* **2014**, *582*, 108−118.
(41) Abdelkader, E. M.; Jelliss, P. A.; Buckner, S. W. Metal and Metal Carbide Nanoparticle Synthesis Using Electrical Explosion of Wires Coupled with Epoxide Polymerization Capping. *Inorg. Chem.* **2015**, *54*, 5897−5906.
(42) Wan, W.; Xiong, J.; Liang, M. Effects of Secondary Carbides on the Microstructure, Mechanical Properties and Erosive Wear of Ti(C,N)-Based Cermets. *Ceram. Int.* **2017**, *43*, 944−952.
(43) Liu, D.; Zhang, A.; Jia, J.; Meng, J.; Su, B. Phase Evolution and Properties of (VNbTaMoW)C High Entropy Carbide Prepared by Reaction Synthesis. *J. Eur. Ceram. Soc.* **2020**, *40*, 2746−2751.
(44) Ye, B.; Wen, T.; Nguyen, M. C.; Hao, L.; Wang, C.-Z.; Chu, Y. First-Principles Study, Fabrication and Characterization of $(Zr_{0.25}Nb_{0.25}Ti_{0.25}V_{0.25})C$ High-Entropy Ceramics. *Acta Mater.* **2019**, *170*, 15−23.
(45) Deng, B.; Wang, Z.; Chen, W.; Li, J. T.; Luong, D. X.; Carter, R. A.; Gao, G.; Yakobson, B. I.; Zhao, Y.; Tour, J. M. Phase Controlled Synthesis of Transition Metal Carbide Nanocrystals by Ultrafast Flash Joule Heating. *Nat. Commun.* **2022**, *13*, 262.

https://doi.org/10.1021/acsomega.3c09045
ACS Omega 2024, 9, 7069−7074